Well log interpolation guided by geologic distance[a]

Yunzhi Shi, Xinming Wu, and Sergey Fomel, The University of Texas at Austin

ABSTRACT

Seismic reflection images can be used to interpolate rock properties between well logs. However, geologic faults may introduce discontinuities that interfere with the interpolation. We propose a modification of an image guided well log interpolation method that incorporates geologic structures including faults and unconformities. We first use predictive painting to spread the lithological information along seismic images from well locations. Then we measure the geologic distance following seismic horizons, and modify the distance across faults during interpolation based on fault attribute measurements. After that, painting interpolation not only honors the seismic horizon structures, but also gets constrained at faults while still remaining effective within the range of conforming regions. Both synthetic and field data examples show a significant improvement in robustness of predictive painting interpolation in complex subsurface structure around fault location.

INTRODUCTION

Well-log properties can be extended to a volume using a 3D seismic image to obtain a global interpretation of the subsurface. Such integration of well log data and seismic images can be used to constrain the following seismic inversion. Beginning with tying well logs measured in depth to seismic data in two-way time (Wu and Caumon, 2016), the joint interpretation requires spatially interpolating and extrapolating the well logs using seismic data. Several authors have studied using post-stack seismic data together with other attributes to guide the interpolation (Taner et al., 1994; Schultz et al., 1994; Hampson et al., 2001), while assuming that the interpolated rock property conforms to seismic horizons.

However, picking seismic horizons can involve manual labor and subjectivity. Hale (2010) proposed the image-guided interpolation of borehole data without picking seismic horizons or faults using the blended neighbor interpolation method (Hale, 2009a). Rather than using only the seismic image structures, Karimi and Fomel (2015) proposed an approach based on predictive painting (Fomel, 2010) that utilizes both image structures and amplitudes to guide the interpolation of well logs.

Although predictive painting can guide the interpolation along conforming horizons, it encounters difficulties in painting across faults or unconformities. Therefore,

it is necessary to limit the interpolation painting only within the range of conforming image structures.

In order to constrain well-log interpolation, seismic coherency attributes can be measured to enhance indistinguishable faults or other geological discontinuities (Chopra and Marfurt, 2005). Many methods were proposed to detect faults and measure fault attributes, including computing normalized cross-correlation (Bahorich and Farmer, 1995), eigenvalues of the local covariance matrix (Gersztenkorn and Marfurt, 1999), eigenvectors of the structure tensor (Randen et al., 2000; Hale, 2009b), and predictive coherency (Karimi et al., 2015). Phillips et al. (2016) proposed a modified Sobel filter that utilizes plane-wave destruction and plane-wave shaping. Wu (2017) recently used directional structure-tensor-based coherence to measure fault likelihood in seismic images.

We propose to apply the fault discontinuity attribute as an additional constraint to assist seismic-guided well-log interpolation. Using this attribute, we modify the distance between seismic traces across the fault, so that the interpolation will not be affected by well logs obscured by the fault but only the well logs that conformally paint at such location. We define geologic distance as the distance measured along seismic horizons. Because geologic distance can better represent the coherence level along seismic horizons than horizontal geometric distance, it provides a more accurate weight for spreading and interpolating well log information.

METHOD

Predictive painting

Predictive painting (Fomel, 2010) spreads the time values along a reference trace into the seismic volume to output the relative geologic time (RGT) attribute. Based on plane-wave destruction method (Fomel, 2002), the predictive painting operator $\mathbf{P}_{r,k}$ is a recursion of multiple operators that predict adjacent traces:

$$\mathbf{P}_{r,k} = \mathbf{P}_{k-1,k}\mathbf{P}_{k-2,k-1}\dots\mathbf{P}_{r+1,r+2}\mathbf{P}_{r,r+1}. \tag{1}$$

Each adjacent prediction follows the local dip patterns $\mathbf{p}_k$ which are defined by plane-wave destruction.

Figure 2 shows an application of predictive painting on the Sigmoid synthetic model (Claerbout, 1992) from Figure 1. While we use the seismic reflection signals to simulate the subsurface model, one of the seismic traces is extracted as a "well log" measurement. With proper sampling and ideal predictive painting based on the seismic image, we can recover the original model, which in this case is the same as the image itself.

However, notice the fault highlighted by the box in Figure 1; predictive painting in Figure 2 failed to capture the discontinuities along seismic horizons.
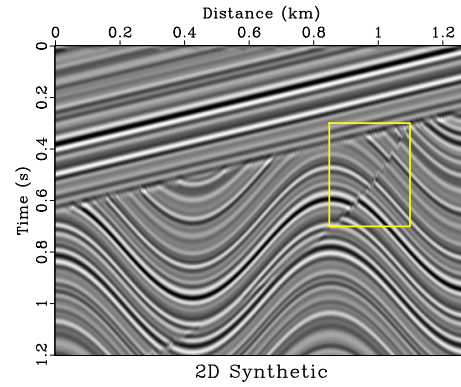
Figure 1: Sigmoid synthetic model, including unconformities and faults. interpfault-sigmoid/ sigmoid
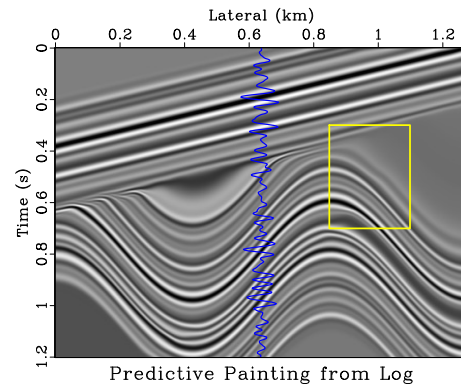

Figure 2: Predictive painting across the seismic image from synthetic well. The well-log synthetic is generated by copying the seismic trace at selected location. interpfault-sigmoid/ paint1

Modified radial basis function interpolation

In order to interpolate the rock properties predicted by several well logs, Karimi and Fomel (2015) used a weighted summation of the painting predictions. The weights were calculated by radial basis function (RBF) $\phi(d) = \phi(|x_k - x_r|)$, whose value decays along the increasing distance (Micchelli, 1984). An inverse quadratic form of the RBF is:

$$\phi(d) = \frac{1}{1 + (d/d_0)^2}, \quad \text{where } d_0 > 0. \tag{2}$$

Then the interpolation can be calculated as below:

$$S(\mathbf{x}) = \frac{\sum_{r=1}^{N} \phi(|x - x_r|) S_r(\mathbf{x})}{\sum_{r=1}^{N} \phi(|x - x_r|)}, \tag{3}$$

where S_r is the result of spreading well log at well location x_r into the seismic data and N represents the total number of used wells.

We propose to extend the definition of d from simply the horizontal distance $|x_k - x_r|$ to the geologic distance that is measured along the seismic horizon:

$$\tilde{d}(\mathbf{x}_k, \mathbf{x}_r) = \int_{\mathbf{x}_r}^{\mathbf{x}_k} \left(\Delta l(\mathbf{x}) + \lambda f(\mathbf{x}) \right) \, d\mathbf{h}(\mathbf{x}), \tag{4}$$

in which $\mathbf{x}_r$, $\mathbf{x}_k$ are points along a seismic horizon $\mathbf{h}(\mathbf{x})$; $\Delta l(\mathbf{x})$ is the curve length of the horizon, it can be calculated by $\Delta l(\mathbf{x}) = \Delta x \sqrt{1 + p^2}$ given local slope estimation p; $f(\mathbf{x})$ is fault attribute and λ represents the distance penalty parameter, this term exaggerates the distance across fault. The geologic distance indicates the decay of information confidence from the reference trace. We perform this integration efficiently by accumulative predictive painting.

NUMERICAL EXAMPLES

Synthetic data test

First of all, we extracted 3 traces from the Sigmoid model at lateral locations 0.09km, 0.64km, and 1.19km. The predictive painting of the trace sampled at 0.64km is shown in Figure 2. Then we compute the interpolation weighted by RBF according to conventional geometric distance $d(x_k, x_r)$, the result is shown in Figure 3a.

Next, we incorporate the proposed $\tilde{d}(\mathbf{x}_k, \mathbf{x}_r)$ in the interpolation for comparison. We measure the fault attribute using plane-wave Sobel filter proposed by Phillips et al. (2016). In result Figure 3b, the recovery at the fault location is significantly improved, because geologic distance weights prevent the well log information from incorrectly spreading across the fault.
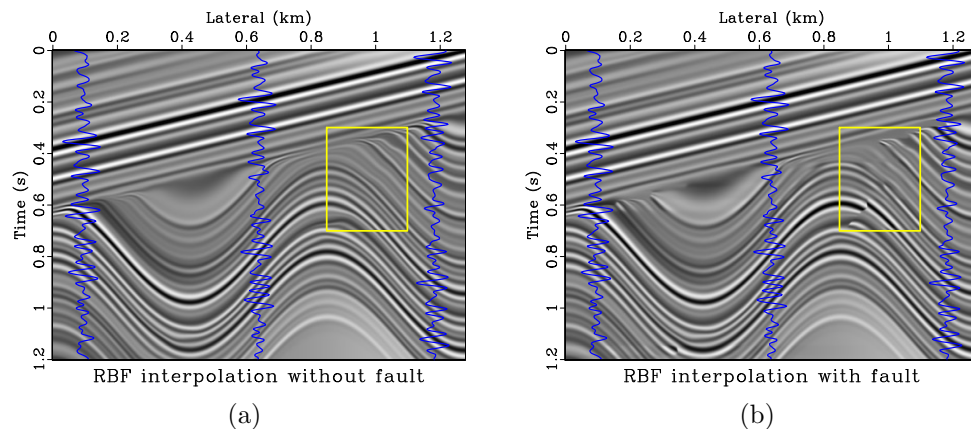
Figure 3: Interpolation results with (a) conventional RBF coefficients without considering faults, and (b) proposed modified RBF coefficients using geologic distance.
interpfault-sigmoid/ interpold,interp

Field data test

We also test the workflow on a field data example collected at Teapot Dome. Figure 4 shows the input seismic section. It is a 2D line extracted from the original 3D data volume which has been converted from time to depth. The seismic image will be used to guide the interpolation of 11 density well logs scattered along the section, they have been tied to the seismic volume using automatic seismic-well tying technique (Wu and Caumon, 2016).
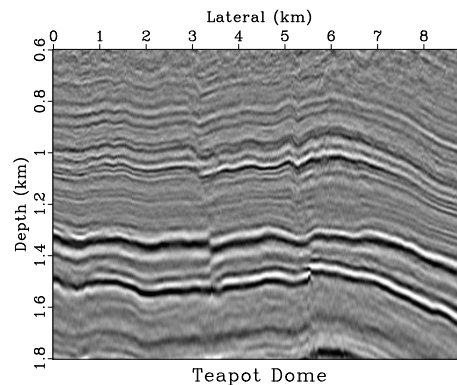

Figure 4: 2D seismic section from Teapot Dome data. The section is extracted from the original 3D data volume along a curve that passes through severa well locations.
interpfault-teapot/ teapot

In this example, we use the method proposed by Wu (2017) based on structure-tensor to measure the fault attribute. It is shown in Figure 5 along with the geologic distance $\tilde{d}$ with regard to a reference well at about 12km. The image shows that at

locations obscured by fault, geologic distance is magnified so that the RBF weight is expected to be suppressed.
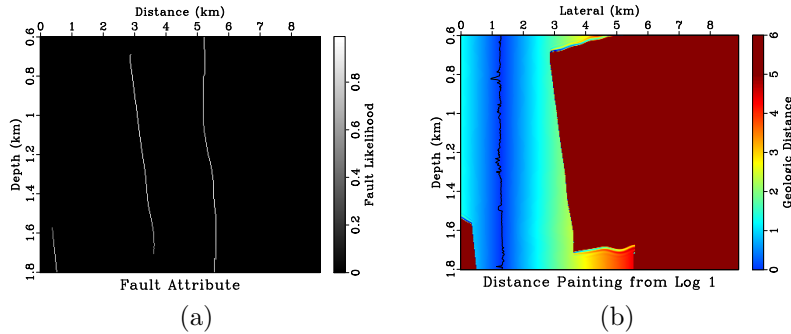

Figure 5: (a) fault likelihood attribute based on structure-tensor method; (b) the geologic distance $\tilde{d}$ computed according to the fault attribute. interpfault-teapot/ fault,dist0

Figure 6 shows the predictive painting from the same well log and its corresponding RBF interpolation weight. Although painting prediction is conforming and smooth, in regions obscured by faults the prediction might be incorrect; however, the interpolation weight at such area will suppress the incorrect painting.
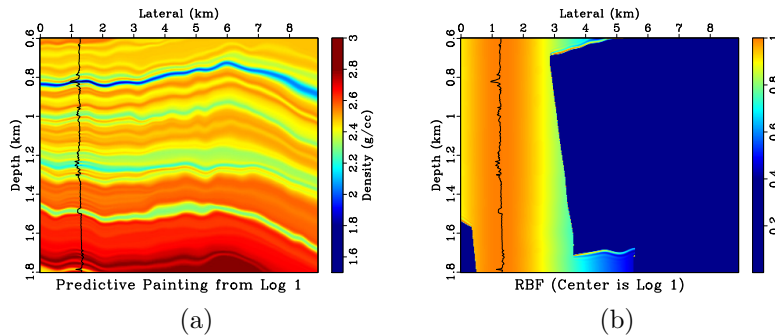

Figure 6: (a) predictive painting from the well log located at about 12km laterally; (b) corresponding RBF weight, which will be used in interpolation later. interpfault-teapot/ paint0,rbf0

Figure 7 shows the geologic distances and corresponding predictive paintings from several other well logs.

The final interpolation of eleven wells are shown in Figure 8.

DISCUSSION

Besides faults, image guided well log interpolation can be also bounded by unconformities when no auxiliary information can be used to continue the interpolation.
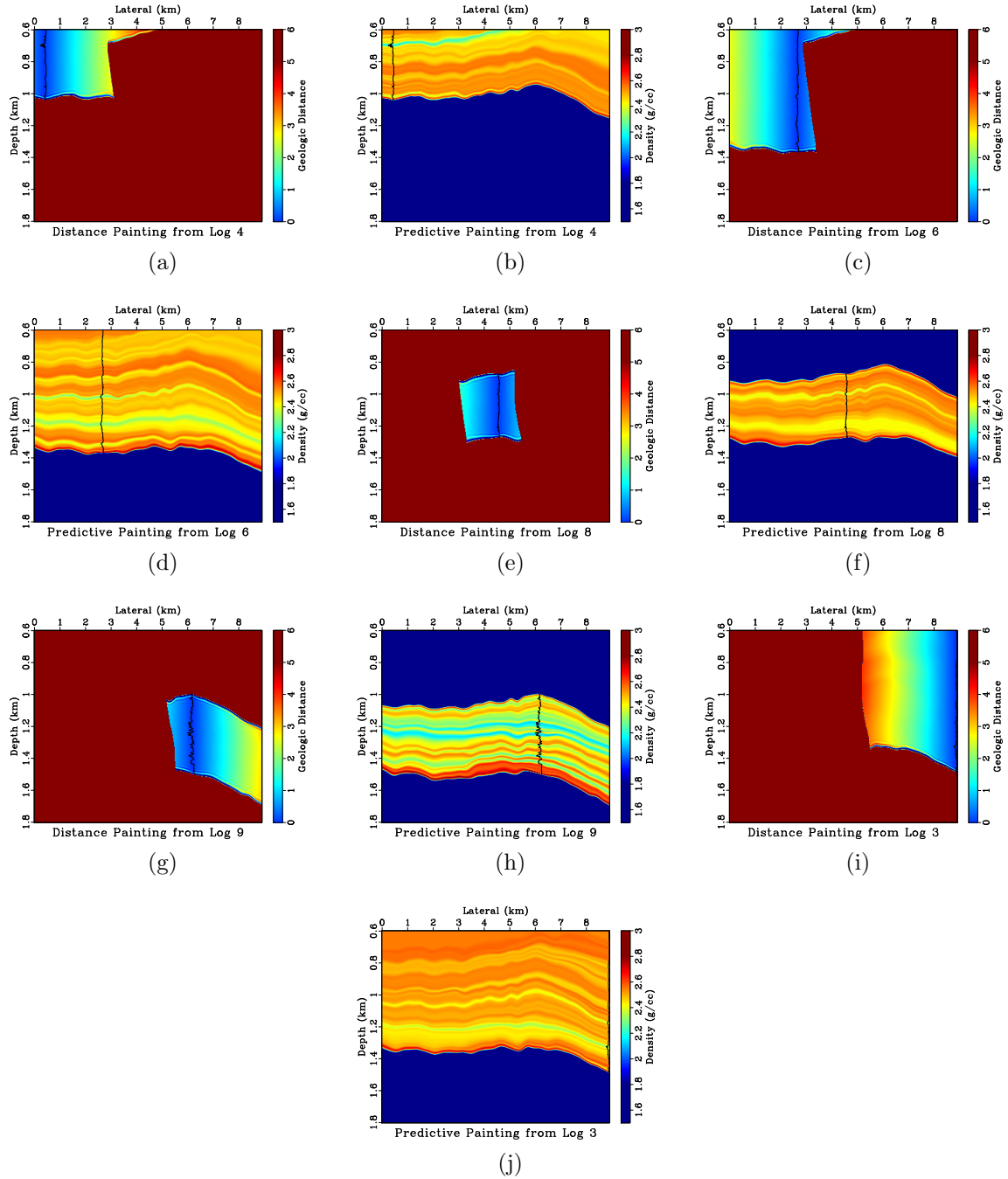
Figure 7: (a,c,e,g,i) geologic distances $\tilde{d}$ and (b,d,f,h,j) the predictive paintings from corresponding well logs guided by the seismic image. interpfault-teapot/ dist3,paint3,dist5,paint5,dist7,paint7,dist8,paint8,dist2,paint2
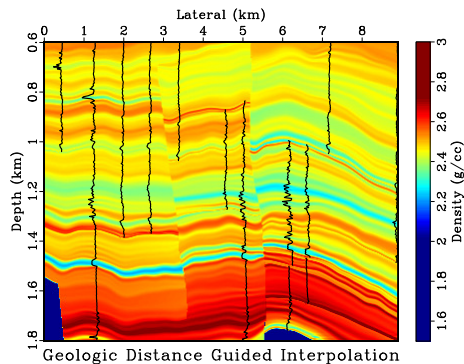
Figure 8: Interpolation result using 11 well logs on Teapot Dome data. interpfault-teapot/ interp-tpt

Proper attributes can help truncate and terminate the unreliable predictive painting at unconformity. Wu and Hale (2015) proposed a 3D unconformity attribute computed from seismic amplitude. Furthermore, further research should focus on how to determine the obscure behavior of faults on the 3D predictive painting extrapolation.

On the other hand, if the offset of the fault is given, Xue et al. (2017) proposed an alternative approach to perform predictive painting across the fault.

CONCLUSIONS

The proposed approach to well-log interpolation provides an effective and efficient method to build a subsurface model that integrates rock property measurements and seismic images while honoring faults and other discontinuities. We have introduced a new definition, geologic distance, to replace the horizontal distance in interpolation. The new representation incorporates more structural information such as seismic horizons and fault attributes. The key benefit of the proposed workflow is the significant improvement of interpolation around fault regions, which is demonstrated in numerical examples. The proposed interpolation can help build correct and robust initial models for further seismic inversion.

ACKNOWLEDGMENTS

REFERENCES

Bahorich, M., and S. Farmer, 1995, 3-D seismic discontinuity for faults and stratigraphic features: The coherence cube: The leading edge, **14**, 1053–1058.

Chopra, S., and K. J. Marfurt, 2005, Seismic attributes – A historical perspective: Geophysics, **70**, 3SO–28SO.

Claerbout, J. F., 1992, Filling data gaps using a local plane-wave model.

Fomel, S., 2002, Applications of plane-wave destruction filters: Geophysics, **67**, 1946–1960.

——, 2010, Predictive painting of 3D seismic volumes: Geophysics, **75**, A25–A30.

Fomel, S., P. Sava, I. Vlad, Y. Liu, and V. Bashkardin, 2013, Madagascar: Open-source software project for multidimensional data analysis and reproducible computational experiments: Journal of Open Research Software, **1**.

Gersztenkorn, A., and K. J. Marfurt, 1999, Eigenstructure-based coherence computations as an aid to 3-D structural and stratigraphic mapping: Geophysics, **64**, 1468–1479.

Hale, D., 2009a, Image-guided blended neighbor interpolation of scattered data: 79th Annual International Meeting, SEG, Expanded Abstracts, Society of Exploration Geophysicists, 1127–1131.

——, 2009b, Structure-oriented smoothing and semblance: Center for wave phenomena: Report CWP-635.

——, 2010, Image-guided 3D interpolation of borehole data: 80th Annual International Meeting, SEG, Expanded Abstracts, Society of Exploration Geophysicists, 1266–1270.

Hampson, D. P., J. S. Schuelke, and J. A. Quirein, 2001, Use of multiattribute transforms to predict log properties from seismic data: Geophysics, **66**, 220–236.

Karimi, P., and S. Fomel, 2015, Image guided well log interpolation using predictive painting: 85th Annual International Meeting, SEG, Expanded Abstracts, Society of Exploration Geophysicists, 2786–2790.

Karimi, P., S. Fomel, L. Wood, and D. Dunlap, 2015, Predictive coherence: Interpretation, **3**, SAE1–SAE7.

Micchelli, C. A., 1984, Interpolation of scattered data: distance matrices and conditionally positive definite functions, *in* Approximation theory and spline functions: Springer, 143–145.

Phillips, M., S. Fomel, and R. Swindeman, 2016, Structure-oriented plane-wave sobel filter for edge detection in seismic images: 86th Annual International Meeting, SEG, Expanded Abstracts, Society of Exploration Geophysicists, 1954–1959.

Randen, T., E. Monsen, C. Signer, A. Abrahamsen, J. O. Hansen, T. Sæter, and J. Schlaf, 2000, Three-dimensional texture attributes for seismic data analysis: 70th Annual International Meeting, SEG, Expanded Abstracts, Society of Exploration Geophysicists, 668–671.

Schultz, P., M. Hattori, P. Mantran, J. Hoskins, C. Corbett, et al., 1994, Seismic-guided estimation of reservoir properties: Presented at the SPE Annual Technical Conference and Exhibition, Society of Petroleum Engineers.

Taner, M. T., J. S. Schuelke, R. O'Doherty, and E. Baysal, 1994, Seismic attributes

revisited: 64th Annual International Meeting, SEG, Expanded Abstracts, Society of Exploration Geophysicists, 1104–1106.

Wu, X., 2017, Directional structure-tensor-based coherence to detect seismic faults and channels: Geophysics, **82**, A13–A17.

Wu, X., and G. Caumon, 2016, Simultaneous multiple well-seismic ties using flattened synthetic and real seismograms: Geophysics, **82**, IM13–IM20.

Wu, X., and D. Hale, 2015, 3D seismic image processing for unconformities: Geophysics, **80**, IM35–IM44.

Xue, Z., X. Wu, and S. Fomel, 2017, Predictive painting across faults: 87th Annual International Meeting, SEG, Expanded Abstracts, submitted.